

Mechanical and dry sliding wear behavior of ultrafine-grained AISI 1024 steel processed using multiaxial forging

A. K. Padap · G. P. Chaudhari · S. K. Nath

Received: 2 December 2009 / Accepted: 18 March 2010 / Published online: 2 April 2010
© Springer Science+Business Media, LLC 2010

Abstract AISI 1024 steel was severely deformed by using warm (500 °C) multiaxial forging (MAF) technique using up to nine forging passes in order obtain a composite ultrafine grained (UFG) microstructure consisting of fragmented cementite particles. Microstructural evolution is studied using optical and electron microscopy. After warm MAF, the hardness and strength properties improved significantly, although total elongation values decreased. The tribological properties of UFG low carbon steel produced by MAF have been investigated. Dry sliding was carried out using constant sliding speed. The wear test results showed that the strengthening of AISI 1024 steel by warm MAF processing did not lead to improvement of wear resistance. The results are explained on the basis of its microstructural features and lower pull-off work. Higher grain boundary density, presence of submicron-sized cementite particles, and lower pull-off work are found to be responsible for lower sliding wear resistance of UFG steel.

Introduction

Ultrafine grained (UFG) materials fabricated by severe plastic deformation (SPD) show improved mechanical and physical properties [1, 2]. Multiaxial forging (MAF) is one of the many SPD techniques used to fabricate UFG materials with improved hardness and strength. As these materials have much higher hardness than that of coarse grained (CG) materials, they are expected to possess higher

wear resistance. These materials might be used as wear resistant parts like molds, bearings, and gears [3].

A few studies have been reported on wear behavior of UFG materials [3–9]. Wear resistance of UFG steel and cp aluminum obtained by equal channel angular processing (ECAP) and accumulative roll bonding (ARB), respectively, was found to be lower than their CG as received materials [4]. In another study on commercial 5052 and 5083 Al alloys refined by ARB to 200-nm grain size, the dry sliding wear resistance of the UFG Al alloys was lower than that of the as-received CG alloys [5]. This was attributed to non-equilibrium and unstable grain boundaries and low strain hardening capability of the UFG alloys. On the other hand, the dry sliding wear resistance of an Al-bronze alloy after equal channel angular extrusion (ECAE) was significantly improved [6]. This was ascribed to improved strength and hardness of the UFG material. Further, the wear mechanism changed from adhesive wear for CG material to abrasive wear for UFG Al bronze. The ECAE processing of Ti improved the strength significantly; however, it had no significant effect on the dry sliding adhesive wear behavior of UFG Ti [7, 8]. On the other hand, in the ECAP-processed UFG Ti, lower adhesion component and consequently lower friction coefficient are reported [9].

As per the above review, some studies suggest that the wear resistance of UFG materials is either unaffected or inferior to that of CG materials. Whereas, other studies have indicated improved wear resistance in UFG materials. Thus, there are contradictory observations on the wear behavior of UFG materials synthesized by SPD techniques. The above review also suggests that the wear behavior of UFG materials processed by SPD techniques may not be generalized and it may be governed by specific alloy system. This aspect needs to be investigated. Moreover, very little work is reported on wear behavior of UFG steels

A. K. Padap · G. P. Chaudhari (✉) · S. K. Nath
Department of Metallurgical and Materials Engineering, Indian Institute of Technology Roorkee, Uttarakhand 247667, India
e-mail: chaudfmt@iitr.ernet.in

produced by SPD techniques and to authors' knowledge, there is no work on UFG steels processed by MAF. Interesting microstructural development is reported on UFG low carbon steel processed by MAF [10] wherein pearlitic cementite lamellae fragmented into nanosized particles dispersed in ferritic matrix. In view of this, it is interesting to conduct a dry sliding wear study on the UFG low carbon steel fabricated by MAF and investigate the reasons for the observed wear behavior. This is the scope of present work.

Experimental procedure

MAF

AISI 1024 steel having chemical composition (wt%) of 0.24 C, 0.5 Mn, 0.05 Si, 0.028 P, and 0.029 S and balance iron is used in this study. Samples were machined into prismatic shape of size 20 mm × 16.33 mm × 13.33 mm. The dimensional ratio of samples for MAF is 1.5:1.22:1.0. All samples were annealed at 920 °C for 60 min to obtain uniform initial microstructure. Successive uniaxial compressions of $\varepsilon = -0.4$ were applied to the longest side at each strain step. Assuming volume conservation and material isotropy, this procedure enables the initial dimensional ratio to be maintained at the end of each pass [11]. Samples were heated at 500 °C before they were alternately forged, after furnace holding time of 50 min, with loading direction changed through 90°. Graphite powder was used for lubrication during forging. At large strains, use of graphite lubrication causes relatively homogeneous deformation [12]. Forging was performed at a strain rate of approximately 10 s⁻¹. Strain in each forging pass was about -0.4. The samples were quickly cooled in water after each pass of forging.

Microstructural characterization

CG-annealed sample was characterized for microstructure using optical microscope Leica DMI 5000 M. UFG material prepared by MAF was observed under a FEI Quanta 200 FEG scanning electron microscope (SEM). A FEI Tecnai 20 G² S-Twin transmission electron microscope (TEM) operated at 200 kV was used for TEM work. Thin foils for TEM investigation were twinjet electropolished in a 10% perchloric acid and 90% glacial acetic acid at room temperature. Surface morphology (2D and 3D) of the worn surfaces was characterized by AFM (NT-MDT, Ntegra) operated in semi contact (tapping) mode. A maximum of 17 μm^2 of specimen area is scanned to calculate the surface roughness values.

Mechanical characterization

Hardness tests were performed using a FIE-VM50 PC Vickers hardness tester by employing 30-kg load. At least five hardness readings were taken and the average is reported along with standard deviation. Tensile tests were performed on the small size samples with 8-mm gauge length and total length of 17 mm [13] using tensile testing machine (H25 K-S Tinius Olsen). The width and thickness were 1.5 and 0.75 mm, respectively.

Dry sliding wear test

Cylindrical pin samples (~20-mm height, 5-mm diameter) were prepared from the annealed material (CG) and the UFG material obtained by MAF (pass 9) technique. Pin samples used for wear tests had flat surfaces in the contact region and were slightly rounded at the corner. These surfaces were polished using 4/0 grade of emery paper followed by cleaning with acetone. A pin-on-disc machine (M/s DUCOM, Bangalore India) fitted with a hardened and polished disc made of En-32 steel (HRC 62–65 hardness) was used as a counter face for dry sliding wear. Pin weight losses were measured at different intervals of sliding time. Weight-loss data were converted to volume-loss data using a value of 0.007858 g/mm³ for density of steel. The pin was removed from the holder after a definite sliding time interval, weighed, and fixed again in exactly the same position in the holder so that the orientation of the pin remains unchanged. Weighing was performed using an electronic balance (Mettler AJ100) having an accuracy of 1×10^{-4} g. The weight of the test pin was measured after intervals of 10, 10, 10, 15, 30, and 45 min of sliding time. A constant sliding speed of 1 ms⁻¹ was used. Pin samples were tested at three normal loads viz. 14.7, 24.5, and 34.3 N. The wear tests were performed in a room having relative humidity of 40–60%, at temperature of 23–25 °C. Worn surfaces of the pins were observed under the SEM and AFM.

Results and discussion

Microstructural evolution

Optical microstructures of samples annealed at 920 °C for 60 min are shown in Fig. 1a and b. It shows equiaxed ferrite grains with pearlite colonies. The average grain size of the annealed steel, determined using linear intercept method is 30 μm . Figure 1b shows a high-magnification micrograph revealing well-aligned lamellae in individual pearlitic colonies in annealed samples. Steel with such microstructure was warm MAFed in steps using up to nine

Fig. 1 Microstructure of CG AISI 1024 steel **a** annealed at 920 °C for 60 min, **b** higher-magnification image showing pearlite colony details

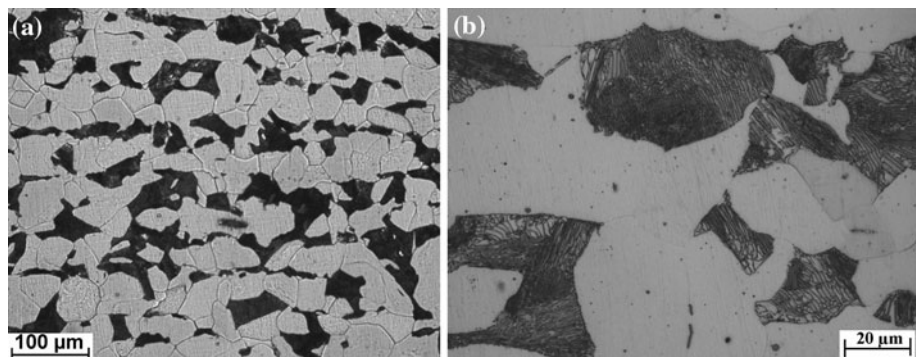
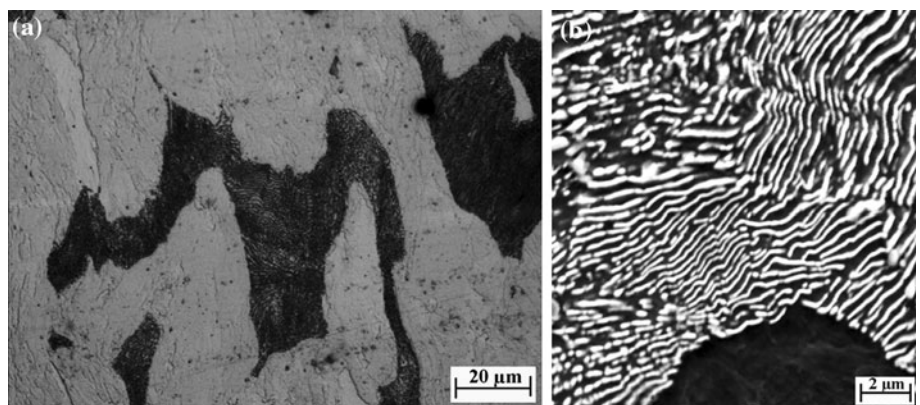


Fig. 2 Microstructure of AISI 1024 steel after six MAF passes **a** optical micrograph showing kink formation and partial fragmentation of pearlitic cementite, **b** higher-magnification SEM image showing similar details in a pearlite colony



forging passes and resulting microstructure was evaluated. After six MAF passes, the changes occurring in the microstructure are revealed in Fig. 2. Severely deformed microstructure shows considerable substructure development in ferrite and pearlitic cementite appears deformed forming kinked patterns (Fig. 2a). Partial fragmentation of cementite has also set in. Fragmentation of cementite is widespread after nine MAF passes. Optical and SEM micrographs of steel sample MAFed using nine MAF passes are shown in Fig. 3a and b, respectively. In this UFG steel, several deformation features are observed in pearlite colonies. It shows extensive fragmentation of pearlitic cementite into ultrafine submicron size particles

that also appear elliptical to spherical in shape in ferritic matrix. Spheroidization of pearlitic cementite is also reported in plain C–Mn steel processed by a four-pass plane strain warm compression process [14]. Therein it was proposed that Spheroidization was accelerated by fragmentation of cementite lamellae and the accompanying pipe diffusion during warm compression. The evolution of spheroidized cementite in MAFed steel is also discussed in detail elsewhere by the authors and is attributed to the change in strain path associated with MAF technique [10]. The role of pearlitic cementite morphology obtained in this work on the adhesive wear will be discussed later in this work.

Fig. 3 Microstructure of UFG AISI 1024 steel after nine MAF passes **a** optical micrograph showing fragmentation of pearlitic cementite, **b** higher-magnification SEM image showing similar details in a pearlite colony

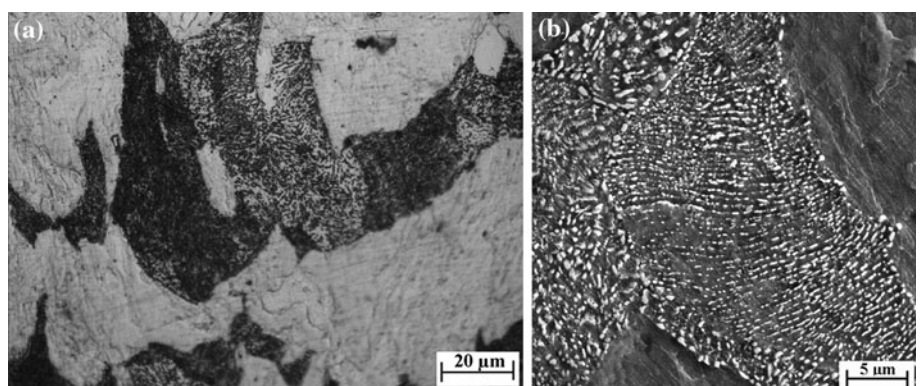


Fig. 4 AISI 1024 steel specimen MAFed using nine MAF passes **a** SEM micrograph showing ferrite grain refinement, **b** bright-field TEM micrograph with SAD pattern (*inset*) showing high misorientation among ferrite grains

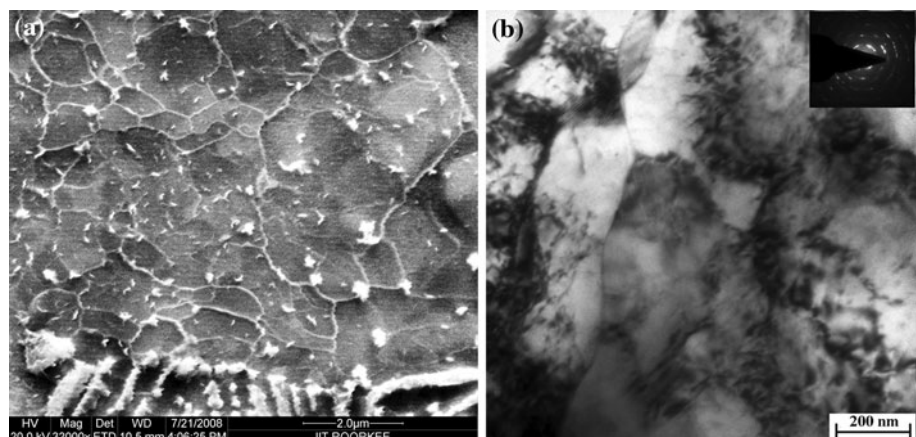


Figure 4a shows SEM micrograph of electropolished steel sample warm MAFed using nine forging passes. It depicts refinement of ferrite grains along with some bordering pearlitic cementite. Comparison with Fig. 1a shows that much of the ferrite phase has refined into well-defined submicron-sized grains. Bright-field TEM micrograph of the specimen MAFed using nine MAF passes is shown in Fig. 4b. The corresponding selected area diffraction pattern (SAED) is shown in the inset. It shows that equiaxed ultrafine grains of average size $0.5 \mu\text{m}$ have been obtained. Some of the grain boundaries are poorly delineated. Inside the grains, the dislocation density is lower, whereas grain boundaries are still associated with high dislocation density. It appears that a recovery process associated with the absorption of dislocations by grain boundaries has set in partially. The associated SAED pattern shows a net pattern suggesting larger misorientations among the finer grains.

Mechanical properties

Often sliding wear behavior of materials is correlated to hardness. Therefore, hardness is measured for differently processed samples. Average Vickers hardness values for the annealed and nine pass MAFed sample are 120 and 253, respectively. Thus, the hardness more than doubled in UFG steel. Figure 5 shows the curves obtained from tensile tests performed on annealed and nine MAF pass samples. The tensile properties are summarized in Fig. 6. It shows the strength and ductility variation after zero and nine MAF passes. After nine MAF passes, the strength doubled while the ductility decreased by more than 50%. This kind of mechanical behavior is typical of most severely deformed metals. Total area under the curves is measured (hatched area) and the values are 1.03 and 0.77 MJ/m^3 respectively, for the CG and UFG steels. This relatively demonstrates that after SPD to produce UFG steel there is a reduction of about 25% in modulus of toughness, although, the hardness and strength increased. The significance of this parameter is discussed in light of wear test results in the following section.

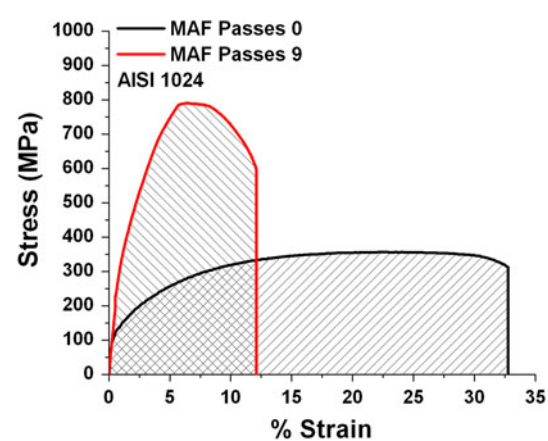


Fig. 5 Tensile curves for AISI 1024 steel showing mechanical behavior of zero MAF pass (annealed, CG) and nine MAF pass (UFG) samples. Area under the curves is represented by *hatched lines*

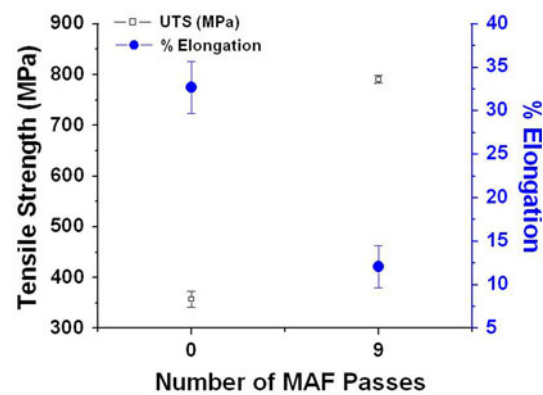
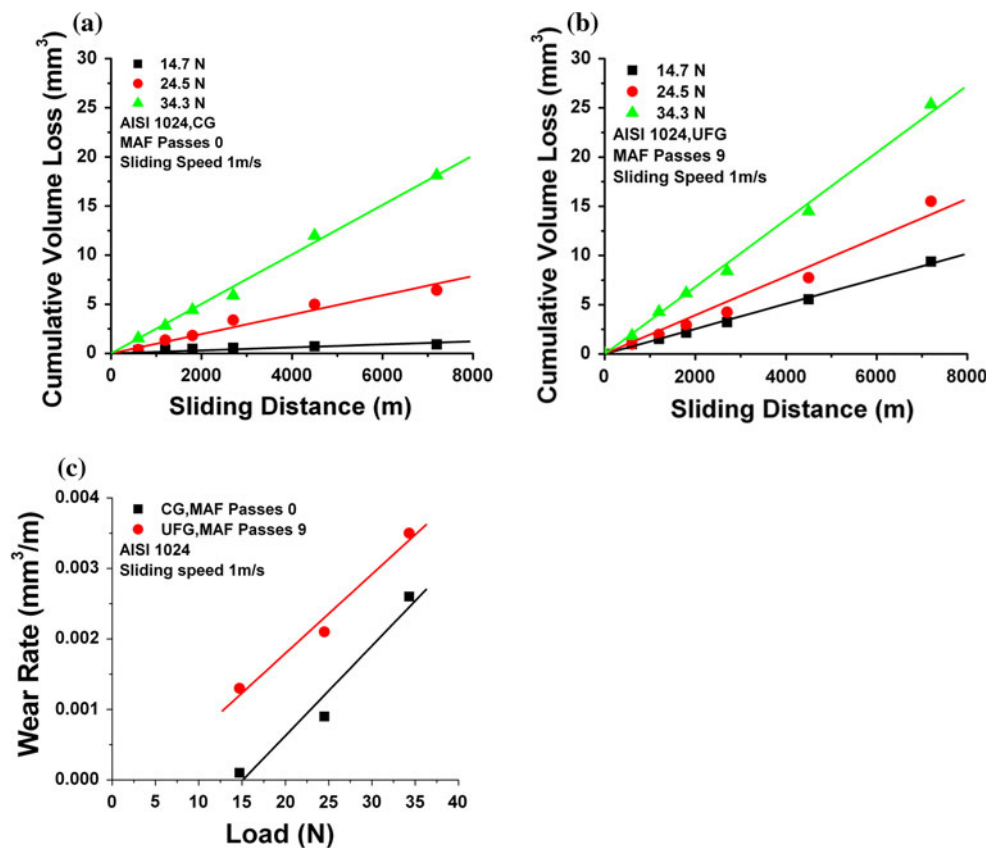


Fig. 6 UTS and ductility (% elongation) for steel MAFed using zero and nine passes

Friction and wear

The variation of wear volume loss as a function of sliding distance, for CG and UFG AISI 1024 steel, is shown in Fig. 7a and b, respectively. It is observed that cumulative

Fig. 7 Variation of cumulative wear volume with sliding distance at different loads **a** CG AISI 1024 steel, **b** UFG AISI 1024 steel fabricated by warm MAF, **c** variation of wear rate with normal load in CG and UFG AISI 1024 steel fabricated by warm MAF



wear volume loss varies linearly with sliding distance for both CG and UFG steel. In both steels, for a given sliding distance, as the normal load increases the cumulative wear volume increases. Thus, cumulative wear volume is least for 14.7 N and is most for 34.3 N normal loads, for any fixed sliding distance. This is in accord with the Archard wear law given below [15].

$$V = \frac{kWS}{H} \quad (1)$$

where V is wear volume loss, S is sliding distance, W is normal load applied, H is hardness of the pin sample, and k is dimensionless Archard wear coefficient.

On comparing Fig. 7a and b, it can be observed that the cumulative wear volume of steel is more in UFG material than the CG material for a constant sliding distance for all the loads, i.e., 14.7, 24.5, and 34.3 N. The wear rate (wear volume/sliding distance, V/S) is calculated from the slope of the linear fit in Fig. 7a and b. Figure 7c shows the variation of wear rate with normal load for both the CG and the UFG steel. It can be observed that wear rate increases linearly with load and it (wear rate) is more for UFG material than for CG steel. The slope of the line in Fig. 7c gives the factor $(V/S) \times (1/W)$. This factor is multiplied by hardness of the sample to yield Archard wear coefficient, k . Table 1 shows the both wear rate and wear coefficient for

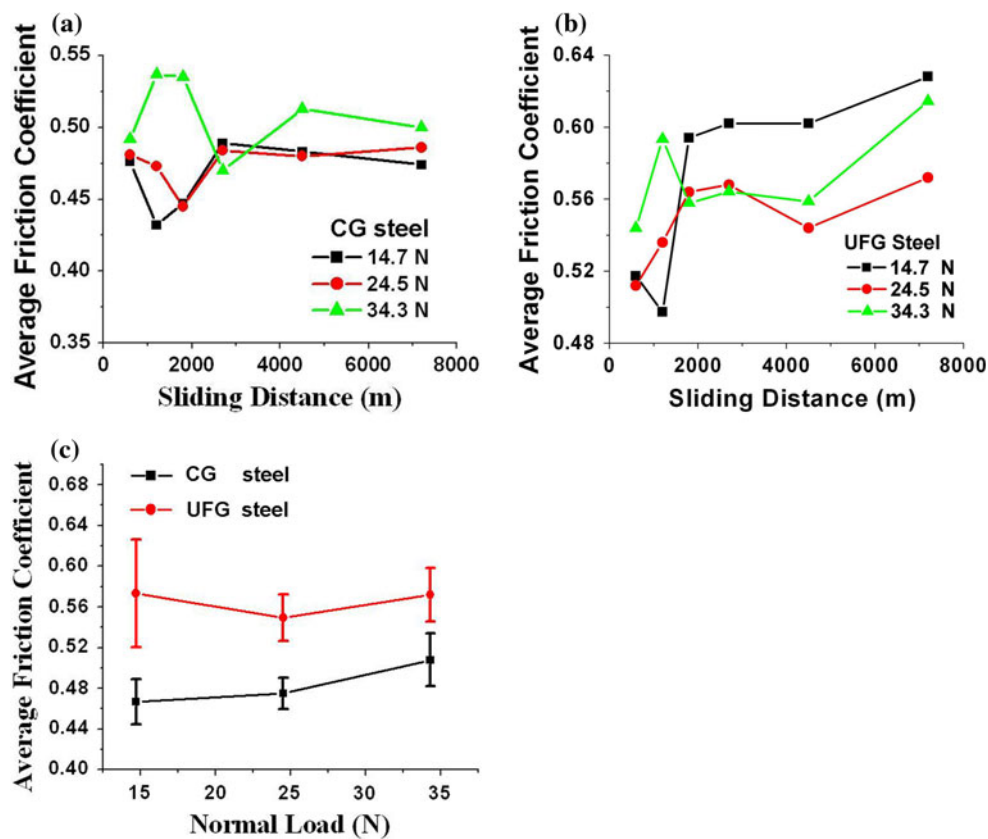
Table 1 Wear rate and wear coefficient for CG and UFG AISI 1024 steel

| AISI 1024 steel | Load | Wear rate (mm^3/m) $\times 10^{-3}$ | Wear coefficient $\times 10^{-4}$ |
|-----------------------|------|---|-----------------------------------|
| CG | 14.7 | 0.1 | 1.18 |
| | 24.5 | 0.9 | |
| | 34.3 | 2.6 | |
| UFG fabricated by MAF | 14.7 | 1.3 | 2.49 |
| | 24.5 | 2.1 | |
| | 34.3 | 3.5 | |

CG as well as UFG steels. The wear coefficient for the CG steel and the UFG steel is found to be 1.18×10^{-4} and 2.49×10^{-4} , respectively.

Figure 8a and b shows the variation of average friction coefficient with sliding distance at different loads. It seems that the fluctuation in the average friction coefficient is more during the initial run in period as compared to steady-state period in both the CG and the UFG steels. During steady state, the friction coefficient for CG steel averages about 0.5, whereas that for UFG steel averages about 0.57. Figure 8c shows the variation of average friction coefficient (during the entire test of 7200 m of sliding distance) with normal load. It is observed that the average friction

Fig. 8 Variation of average friction coefficient with sliding distance at different loads in AISI 1024 steel **a** CG and **b** UFG steel fabricated by warm MAF, **c** variation of average friction coefficient with normal load in CG and UFG steel fabricated by warm MAF

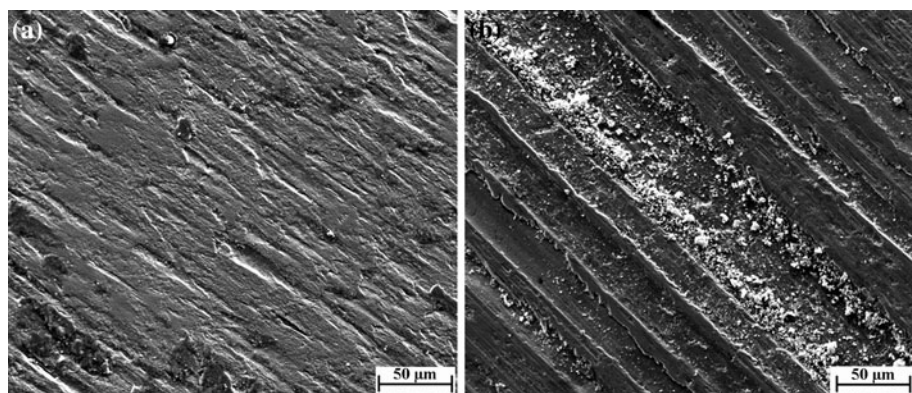


coefficient varies very little with normal load, and its value for UFG steel is higher than that for CG steel for all the three loads.

To correlate the wear test results to the worn surface of the test pins, SEM and AFM techniques are employed. Scanning electron microscopy images have inherently higher depth of field and it can scan larger areas which is extremely useful for topographic studies. However for quantification of surface roughness AFM study is performed. Figure 9a and b shows the SEM micrographs of surfaces of test pins of CG and UFG steels after wear tests are performed. It is clear that the UFG steel has deeper and

wider scratches than the CG steel. The deeper grooves suggest increased metallic contact. This results in higher coefficient of friction [15]. Atomic force microscopy of the worn surfaces confirmed the finding from SEM. Figures 10 and 11 show the AFM images of worn surfaces of CG and UFG steel samples, respectively. The wear grooves are not conspicuous because of smaller sampling area. 2D and 3D images of worn surfaces of CG steel subjected to 14.7 and 34.3 N are shown in Fig. 10a, b and c, d, respectively. Corresponding surfaces for UFG steel are shown in Fig. 11a, b and c, d, respectively. It is evident that the grooves on the surfaces are deeper for UFG steel as compared to CG steels for similar loads.

Fig. 9 SEM micrographs of worn surfaces of test pin after sliding for 7200 m at 1 ms^{-1} under 14.7 N load. **a** CG steel, **b** UFG steel fabricated by MAF. Worn UFG steel exhibits deeper grooves



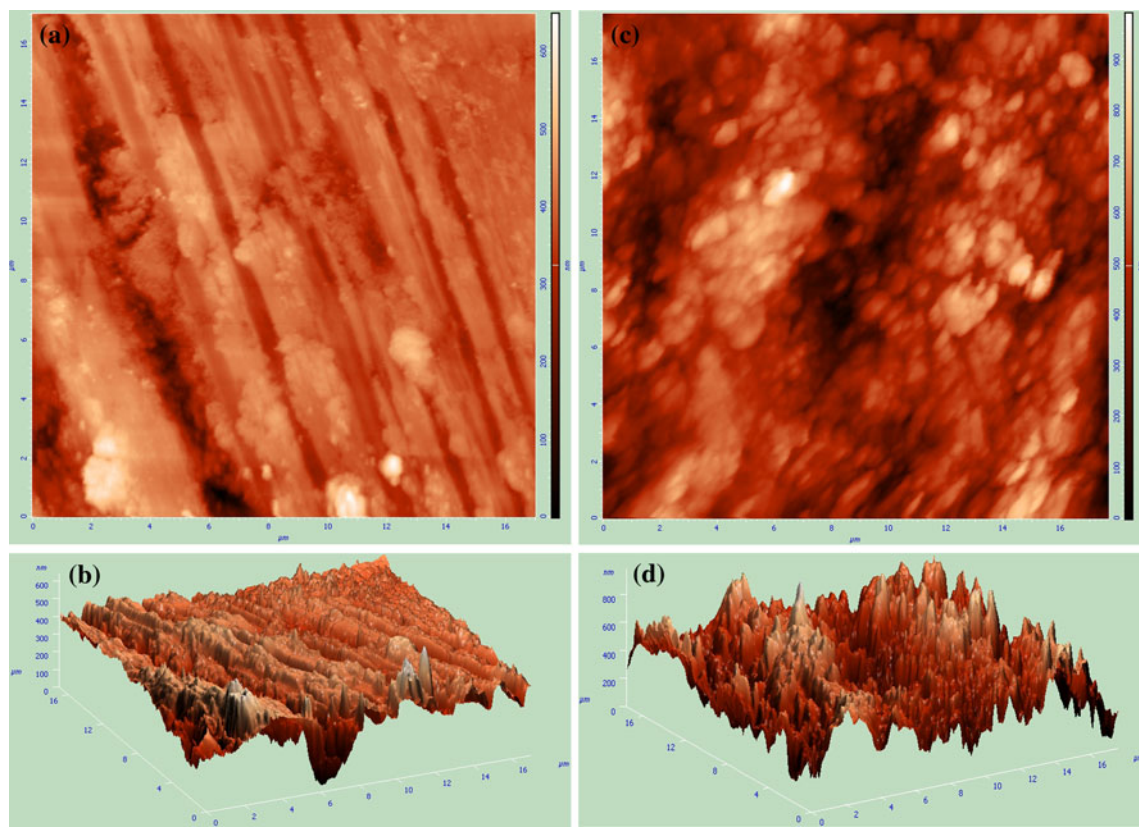


Fig. 10 AFM 2D and 3D images of worn surfaces of CG AISI 1024 steel. **a, b** 14.7-N load, **c, d** 34.3-N load

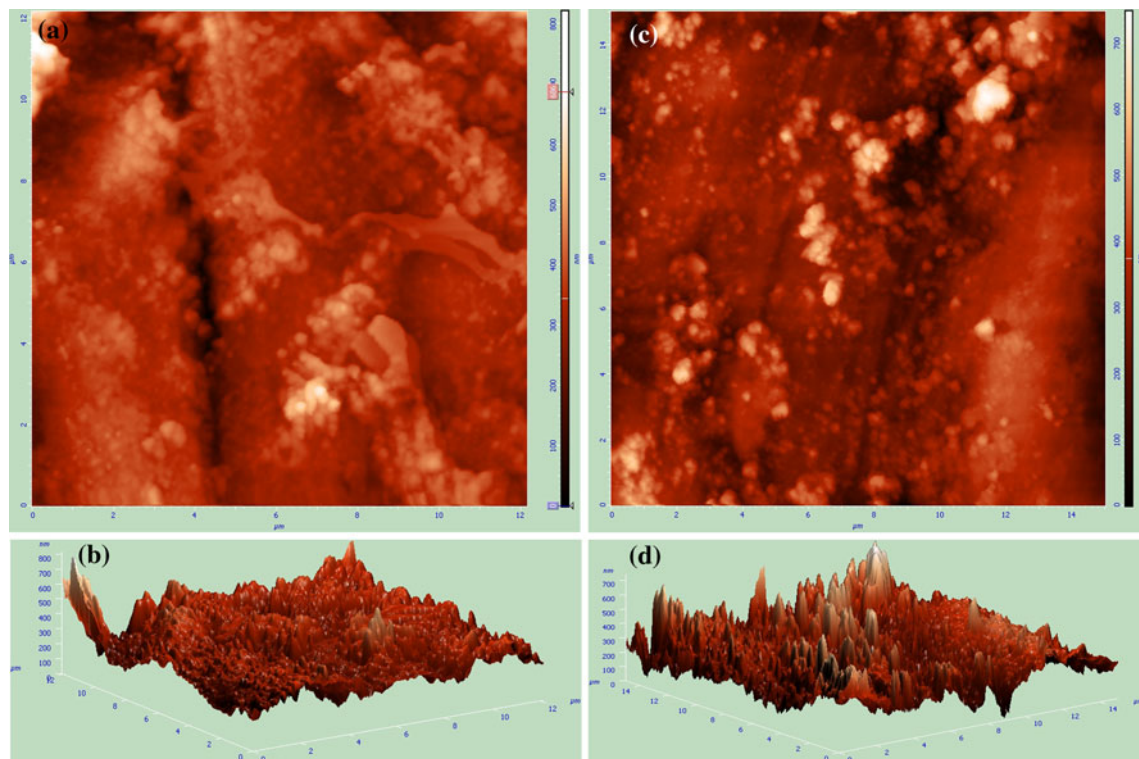


Fig. 11 AFM 2D and 3D images of worn surfaces of UFG AISI 1024 steel. **a, b** 14.7-N load, **c, d** 34.3-N load

Table 2 Roughness values estimated using AFM study of worn surfaces of coarse grained (CG) and ultrafine grained (UFG) steel samples

| AISI 1024 steel, condition of samples and applied load (N) | Roughness, root mean square values (nm) |
|--|---|
| CG, 14.7 | 59.5 |
| CG, 34.3 | 94.5 |
| UFG, 14.7 | 71.1 |
| UFG, 34.3 | 111.9 |

Quantitative analysis of surface roughness in terms of root mean square value of roughness is summarized in Table 2. Surface roughness values for UFG steel are higher than that for the CG steels at all the test loads employed in this study. Higher surface roughness is indicative of increased friction between the pin sample and the counter face. This is also confirmed from the observed higher value of average friction coefficient of 0.57 for UFG steel. Thus, worn surface morphology and observed higher average friction coefficient confirms the observed experimental data that UFG steel has higher wear rate. XRD patterns of the wear debris after zero and nine MAF passes processing of steel are shown in Fig. 12. Same oxide peaks obtained in both the cases suggest the same oxidative wear mechanism in both the steels.

The increase in wear coefficient and wear rate of the UFG steel fabricated by warm MAF is mainly due to the microstructural changes caused during the grain refinement process and the resulting mechanical properties. The higher wear rates in UFG steel are explained in terms of microstructural features and the “pull-off” work as follows. In general, materials with higher grain boundary densities exhibit higher wear rates than those with lower grain boundary densities or single crystals [16]. Grain boundaries are said to influence adhesion, friction, surface fracture, and wear [16]. The microstructural changes occurred in this study included refinement of ferrite grains from 30 μm to submicron-sized grains and fragmentation and spheroidization of pearlitic cementite to submicron to nanoscale dimensions. It is reported that in AISI 1045 spheroidized

steel, the spheroidized cementite in ferrite matrix lowered the wear resistance [17]. The spheroidized cementite was said to nucleate cracks easily in the subsurface and thus enhance the wear. In this study, submicron scale cementite particles were observed in the UFG steel which could nucleate subsurface cracks and this must be one of the reasons responsible for the increased wear.

Further, upon MAF although the strength and hardness of the UFG steel increased, the wear volume did not decrease. If we consider that the adhesive wear is governed by Eq. 1, then it is expected that the wear volume should decrease with increase in hardness in UFG steel. However, the obtained results show just the opposite trend. Thus, improvement in mechanical properties in terms of strength and hardness after SPD processing need not reflect in similar benefits in wear properties. In other words, generalized wear behavior should not be expected of UFG materials synthesized with SPD techniques. With regard to mechanical properties, the inferior adhesive wear resistance of UFG steels can be further explained on the basis of pull-off work. The pull-off work involved in generating the wear particles is a function of area under the stress strain curve of the material [18]. In UFG steel, although the strength increased, the total elongation decreased substantially (Figs. 5, 6) and hence area under the stress-strain curve decreased. Thus, pull-off work in UFG steel is lower than that in CG steel. This caused increased wear in UFG steel processed in this work. If % elongation values of the UFG steel could be improved by subsequent controlled annealing treatment without compromising the strength much then it is likely that improved sliding wear behavior will be obtained.

Conclusions

- (1) Warm MAF of low carbon steel resulted in UFG microstructure. After nine MAF passes, the hardness of steel increased from 120 to 253 VHN. The strength increased from 350 to 800 MPa, whereas elongation decreased from about 33 to 12%.
- (2) The average friction coefficient of UFG steel is higher (0.57) than that of CG steel (0.50). Average friction coefficient did not vary much with applied normal load.
- (3) The Archard wear coefficient for UFG steel is 2.49×10^{-4} , whereas for CG steel 1.18×10^{-4} . Thus, higher wear is observed in UFG steel. The worn surface of UFG steel revealed deeper and wider grooves and more metallic areas as compared to CG steel which showed shallow grooves.
- (4) Adhesive wear behavior of UFG materials processed by SPD techniques can not be generalized, and is

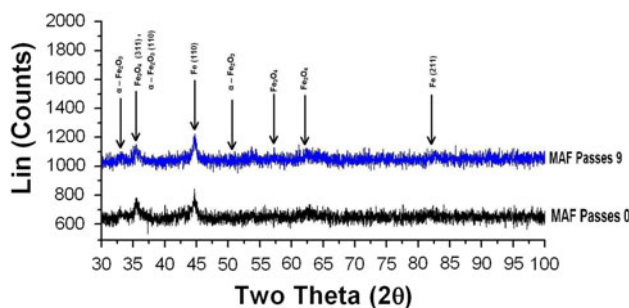


Fig. 12 XRD patterns of wear debris from zero to nine MAF pass samples

specific to the alloy system and microstructural development during deformation processing. Presence of spheroidized nano- and micro-particles of cementite in ferrite matrix and observed lower pull-off work are responsible for the enhanced wear of UFG steel.

Acknowledgements All India Council for Technical Education supported one of the authors at IIT Roorkee under its QIP scheme. Authors gratefully acknowledge the funding provided through the faculty initiation grant of Indian Institute of Technology Roorkee.

References

1. Belyakov A, Sakai T, Miura H, Kaibyshev R (2000) *Scripta Mater* 42:319
2. Valiev RZ (1997) *Mater Sci Eng A* 234–236:59
3. La PQ, Ma JQ, Zhu YT, Yang J, Liu W, Xue Q, Valiev R (2005) *Acta Mater* 53:5167
4. Kim YS, Lee T, Park KT, Kim WJ, Shin DH (2002) TMS (UFG materials II, proceeding of a symposium, TMS annual meeting)
5. Kim YS, Ha JS, Shin DH (2005) *Mater Sci Forum* 475–479:401
6. Gao LL, Cheng X (2008) *Wear* 265(7–8):986
7. Garbacz H, Gradzka-Dahlke M, Kurzydłowski K (2007) *Wear* 263:572
8. Purcek G, Saray O, Kul O, Karaman I, Yapici G, Haouaoui M, Maier H (2009) *Mater Sci Eng A* 517:97
9. Stolyarov VV, Shuster LS, Migranov MS, Valiev RZ, Zhu YT (2004) *Mater Sci Eng A* 371:313
10. Padap AK, Chaudhari GP, Nath SK, Pancholi V (2009) *Mater Sci Eng A* 527:110
11. Lim SM, Wahabi ME, Desrayaud C, Montheillet F (2007) *Adv Mater Res* 5–17:900
12. Salishchev GA, Valiakhmetov OR, Galeev RM (1993) *J Mater Sci* 28:2898. doi:[10.1007/BF00354692](https://doi.org/10.1007/BF00354692)
13. Hyde TH, Sun W, Williams JA (2007) *Int Mater Rev* 52:213
14. Song R, Ponge D, Raabe D, Kaspar R (2005) *Acta Mater* 53:845
15. Hutchings IM (1992) Tribology: friction and wear of engineering materials. Edward Arnold, London, pp 26–83
16. Bhushan B (2002) Introduction to tribology. Wiley, New York, p 345
17. Wayne S, Rice S, Minakawa K, Nowotny H (1983) *Wear* 85:93
18. Arnell RD, Davies PB, Halling J, Whomes TL (1991) Tribology principles and design application. Springer, New York, p 46